Eddy Genesis and Transformation of Stokes Flow in a Double-Lid-Driven Cavity. Part 2: Deep Cavities

F. GÜRCAN[1], M. C. T. WILSON[2] and M. D. SAVAGE[3]
[1]Department of Mathematics, Erciyes University, Kayseri, Turkey
[2]School of Mechanical Engineering, The University of Leeds, Leeds LS2 9JT, UK
[3]Department of Physics and Astronomy, The University of Leeds, Leeds LS2 9JT, UK

Abstract

This paper extends an earlier work [Gürcan *et al.*, *Proc. Instn. Mech. Engrs, Part C: J. Mech. Eng. Sci.*, 2003, **217**, 353] on the development of eddies in rectangular cavities driven by two moving lids. The streamfunction describing Stokes flow in such cavities is expressed as a series of Papkovich-Faddle eigenfunctions. The focus here is deep cavities, i.e. those with large height-to-width aspect ratios, where multiple eddies arise. The aspect ratio of the fully developed eddies is found computationally to be 1.38 ± 0.05, which is in close agreement with that obtained from Moffatt's [*J. Fluid Mech.*, 1964, **18**, 1] analysis of the decay of a disturbance between infinite stationary parallel plates. Extended control space diagrams for both negative and positive lid speed ratios are presented, and show that the pattern of bifurcation curves seen previously in the single-eddy cavity is repeated at higher aspect ratios, but with a shift in the speed ratio. Several special speed ratios are also identified for which the flow in one or more eddies becomes locally symmetric, resulting in locally symmetric bifurcation curves. By superposing two semi-infinite cavities and using the constant velocity damping factor found by Moffatt, a simple model of a finite multiple-eddy cavity is constructed and used to explain both the repetition of bifurcation patterns and the local symmetries. The speed ratios producing partial symmetry in the cavity are shown to be integer powers of Moffatt's velocity damping factor.

Keywords: fluid mechanics, flow structure, bifurcation, stagnation point, Moffatt eddy

Notation

A	cavity aspect ratio $= H/L$
A^*	a critical aspect ratio
A_n, B_n	streamfunction expansion coefficient
A_{eddy}	aspect ratio of fully developed eddies
H	half cavity height (m)
L	half cavity length (m)
n	summation index
N_e	number of complete eddies within the cavity
s_n	streamfunction expansion eigenvalues
S	speed ratio, $= U_1/U_2$
S^*	a critical value of speed ratio
S_i^-	negative speed ratio producing local symmetry
S_i^+	positive speed ratio producing local symmetry
U_1, U_2	top and bottom lid speeds respectively (m/s)
$\mathbf{v}$	dimensionless fluid velocity
$\mathbf{x} = (x, y)$	dimensionless cartesian coordinates
(X, Y)	dimensional cartesian coordinates (m)
ϕ_1^n	streamfunction expansion eigenfunctions
ψ	streamfunction
σ	velocity damping factor

1 Introduction

Cavity type flows are often encountered in the manufacturing and processing industries. Examples include coating flows [1,2], polymer melts [3], ceramic type casting [4] and certain aerodynamics applications [5]. Also, apart from their practical relevance, such flows have proved to be a fertile topic for fundamental study since they exhibit complex flow behaviour in simple geometries [6].

Although the most widely studied cavity flow appearing in the literature is that inside a rectangular domain where the liquid is enclosed by solid walls with one moving lid, very few studies have appeared on a double-lid driven cavity with lids moving either in the same or opposite directions. The few examples include Weiss and Florsheim [7] who considered the symmetric case $S = U_1/U_2 = 1$, where U_1 and U_2 are the lid velocities and S is the speed ratio. Subsequently, Sturges [8] considered the case $S = -1$, where the walls move in opposite directions, and determined streamline structures as the cavity aspect ratio A (depth to width) was varied. Chien *et al.* [9] investigated flow structures experimentally and also numerically using a finite element method. Jana *et al.* [10] used a finite difference method to determine streamline patterns and the number of eddies in the cavity for $0.1 < A < 10$ and $-1 \leqslant S \leqslant 1$. However, they did not determine the degenerate critical points and hence no bifurcation curves in the control space diagram were presented. Recently, Gürcan *et al.* [11] investigated streamline topologies near a non-simple degenerate critical point close to

a stationary wall for a double-lid-driven cavity using both analytic solutions and methods from non-linear dynamical systems.

In the precursor to the present work (henceforth referred to as 'Part 1'), Gürcan *et al.* [12] described the generation of eddies in the double-lid-driven cavity as aspect ratio increases for different speed ratios. They showed that the mechanism by which eddies are formed involves the appearance of side-eddies on the cavity walls and the subsequent interaction of critical streamlines and stagnation points. A particular region of the (S, A) parameter space (namely $-1 \leqslant S < 0$ and $0 < A < 3.2$) was chosen to construct a control space diagram which exhibited several curves representing flow bifurcations at degenerate critical points. These bifurcations were described and interpreted in the context of [13-15] who used methods from nonlinear dynamics to analyse and classify critical points arising in two dimensional, incompressible, viscous flows near to and away from boundaries. The eddy generation process described in Part 1 (where one eddy becomes three) will for convenience be referred to as the 'first phase' of eddy generation.

The present study explores the eddy generation process further by considering cavities with larger aspect ratios — i.e. deep cavities — and also both negative and positive speed ratios. As indicated at the end of Part 1, fully-developed eddies within the deeper cavities can be considered as 'sub-cavities' bounded above and below either by one of the lids or by a separating streamline. When the aspect and speed ratios of a given sub-cavity match critical values found in Part 1 for the single-eddy cavity, the flow bifurcations associated with the first phase of eddy generation should be repeated in the relevant sub-cavity. An extended control space diagram is presented in section 3, which shows that this is indeed the case, and the sub-cavity idea is used to explain certain features of the bifurcation curves by exploiting some results from Moffatt's famous paper on viscous and resistive eddies [16].

2 Boundary value problem

As explained in Part 1, Stokes flow in a lid-driven cavity with two solid walls lying along $X = \pm L$ and two moving lids lying along $Y = \pm H$, is governed by the biharmonic equation for the streamfunction ψ

$$\nabla^4 \psi = 0. \tag{1}$$

Lengths are non-dimensionalised with respect to L such that the flow domain is given by $|x| \leqslant 1$, $|y| \leqslant A$. The streamfunction is set equal to zero on the boundaries of the closed domain, and the no-slip conditions for the upper and lower lids and side walls are

$$\frac{\partial \psi}{\partial y}\,(x, A) = S \ , \ \frac{\partial \psi}{\partial y}\,(x, -A) = 1, \tag{2}$$

$$\frac{\partial \psi}{\partial x}\,(1, y) = \frac{\partial \psi}{\partial x}\,(-1, y) = 0. \tag{3}$$

Following Joseph and Sturges [17] and Gürcan *et al.* [12], the streamfunction for any value

of S can be written as:

$$\psi = \sum_{n=-\infty}^{\infty} \{A_n e^{s_n(y-A)} + B_n e^{-s_n(y+A)}\} \frac{\phi_1^n(x, s_n)}{s_n^2}, \tag{4}$$

where A_n and B_n are complex coefficients determined using a truncation technique [18]. The s_n are complex eigenvalues and the functions ϕ_1^n are even Papkovich-Faddle eigenfunctions, satisfying the no-slip boundary conditions on the side walls. When the coefficients have been determined, the streamfunction at any interior point in the liquid is obtained by simply summing a finite number of terms in the series (4) while ensuring that the magnitude of the truncation error is acceptably small, see Part 1.

3 Eddy genesis when lids move in opposite directions

For each combination of the physical parameters S and A, there is a corresponding unique solution of equation (1) describing the flow. However, the number and type of stagnation points in the flow will vary with S and A. It is important to point out that here the term 'bifurcation' refers to changes in the number or type of stagnation points as S and A are changed.

3.1 Extended control space diagram

In Part 1, the 'first phase' of eddy generation was described, i.e. flow bifurcations were explored for aspect ratios in the range $0 < A < 3.2$, over which the single eddy present at small A is transformed into three complete eddies. Figure 1 shows an extended control space diagram, which has the same range of speed ratio ($-1 \leqslant S < 0$), but covers aspect ratios up to 6. The bottom part of the figure shows again the bifurcation curves IS_1, SE_1, TR_1, SC_1, SC_2 and SN_1 corresponding to the first phase, and the bifurcation or stage of flow transformation represented by each curve is summarised in table 1. The key stages of eddy development are the appearance of an interior saddle point, the appearance of side eddies on the cavity walls, the connection of the side eddies with the interior saddle, and the disappearance of a double-eddy substructure inside one of the two new eddies. The order in which these stages occur depends on the speed ratio, and for certain values of S, secondary bifurcations also occur, such as saddle-node bifurcations away from the centreline.

The upper part of figure 1 ($3.2 < A < 6$) shows the 'second phase' of eddy generation. A striking feature of this extended diagram is that not only do the same flow transformations arise in the second phase, but the entire pattern of the first-phase curves is repeated almost exactly in the second phase (see the shaded portion). The curves $IS_2, SE_2, TR_2, SC_3, SC_4$ and SN_2 represent the same stages of development as appear in the first phase; see table 1. When S is fixed and A increases, crossing the second-phase curves results again in the generation of two new eddies, increasing the number of complete eddies from three to five.

Bifurcation curve	Bifurcation/Stage of development
IS_1 and IS_2	cusp bifurcation creating interior saddle on $x = 0$
SE_1 and SE_2	appearance of side eddies (side-eddy bifurcation) on the walls
TR_1 and TR_2	saddle-point-triangle configuration
SN_1 and SN_2	two saddle-node bifurcations on $x \neq 0$
$SC_i (i = 1, 2, 3, 4)$	transformation from centre to saddle or vice-versa

Table 1: Descriptions of bifurcation curves

This pattern repetition at a shifted speed ratio was anticipated at the end of Part 1, and is explored further in the following section.

The unshaded portion of the second phase shows a new pattern of bifurcation curves exhibiting three local symmetries at $S = S_0^- = -1$, $S = S_1^- = -2.84 \times 10^{-3}$ and $S = S_2^- = -8.5 \times 10^{-6}$. (Note that the superscript minus signs are used to distinguish these significant speed ratios from their $S > 0$ equivalents, which are discussed later.) It is not surprising that the bifurcation curves appear symmetric at $S = -1$, since this is the only speed ratio to produce wholly symmetric flow within the cavity. This means that the flow transformations of the second phase all occur within the middle eddy, with the upper and lower fully-developed eddies remaining unaffected (see schematics on $S = -1$ in figure 1). The symmetry in the middle eddy also affects the type of bifurcation that can occur. In most cases, the creation of the interior saddle point is via a saddle-node (cusp) bifurcation on $x = 0$ above or below the elliptic point at the heart of the eddy. This results in the appearance of two new stagnation points in the flow where there were none before. In the symmetric case, however, the interior saddle point can only appear at the centre of the eddy, i.e. at the elliptic point. Therefore in this case the interior saddle is created via a pitchfork-type bifurcation in which the elliptic point becomes hyperbolic and two new elliptic points are created, which move apart symmetrically above and below the saddle point as A increases. The occurrence of the second-phase pitchfork bifurcation is labelled P_2 in figure 1; the equivalent event in the first phase occurs at P_1.

When $S = S_2^- = -8.5 \times 10^{-6}$ and A increases from 3.0, the bifurcation curves are crossed in the same order as when $S = -1$, and at almost the same aspect ratios: $A = 3.671$ (cf 3.670 when $S = -1$), $A = 5.295$ (5.293), $A = 5.581$ (5.580), and $A = 5.712$ (5.710). The only difference is that the flow transformations occur in the upper eddy, with the middle and lower eddies remaining unaffected. The shift of the development to the upper eddy is because this value of speed ratio no longer produces a global symmetry in the cavity, but instead creates locally symmetric flow conditions in the upper eddy. This is demonstrated by the streamline plots in figure 2. In plot (b), where $S = S_2^-$, the speed along the centre of separating streamline 'I' is equal to the lid speed and the flow is symmetric about the interior saddle point, save for the curvature of streamline 'I'. The other plots show speed ratios above and below S_2^-, and the corresponding asymmetry of the flow in the upper portion of the cavity. Note that the partial symmetry when $S = S_2^-$ also means that for this value of S the interior saddle point is created by means of a pitchfork-type bifurcation as in the $S = -1$ case. This event is labelled P_1^* in figure 1.

The similarity in the aspect ratios at which the bifurcations arise when $S = -1$ and S_2^- is due to the remarkably constant value of the aspect ratio of the fully-developed eddies, which remains essentially unchanged even when new eddies are being created in parts of the cavity. By considering the positions at which the dividing streamlines cross the centreline ($x = 0$) for various combinations of A and S, the value of the fully-developed eddy aspect ratio found computationally is $A_{eddy} = 1.38 \pm 0.05$. Given that A_{eddy} varies so little, it is interesting to try to predict the critical aspect ratios for the second phase of eddy generation by accounting for the presence of two passive eddies in the cavity. In the first phase, at $S = -1$ the critical aspect ratios corresponding to the four stages of flow development are 0.931, 2.498, 2.789 and 2.910. Adding $2A_{eddy}$ to these yields values 3.691, 5.258, 5.549 and 5.670, which differ from the actual values quoted above by less than 1%. This indicates, as one might expect, that bifurcations and key flow structures will arise within a particular eddy of a multi-eddy cavity when the aspect and speed ratios associated with that eddy match those found in Part 1 for the single-eddy cavity. For example, a pitchfork bifurcation will occur in any eddy whose flow is symmetric and whose aspect ratio is 0.93, though why this particular aspect ratio is significant is not yet understood. The above relationship between the first and second phase critical aspect ratios holds across the range of speed ratios, and is one reason why the pattern of the first phase bifurcation curves is repeated in the second phase.

Since the second-phase flow transformations at $S = -1$ and $S = S_2^-$ occur in different eddies, there must be an intermediate speed ratio which marks the shift of activity from one eddy to the other. This is $S = S_1^- = -2.84 \times 10^{-3}$, about which the curves in figure 1 are again locally symmetric. The pattern of bifurcation curves is also more intricate here, and since this structure was not seen in Part 1, an enlarged view of this part of control space is given in figure 3. The flow development sequence is more complicated in this region due to the appearance of saddle-node bifurcations away from the centreline, which result in the creation of off-centre saddle points and associated homoclinic streamlines defining small interior eddies. However, the schematics in figure 3 show that to the left of S_1^- the middle eddy is the focus of eddy generation, while to the right it is the upper eddy.

When $S = S_1^-$, as shown in figure 4, the upper and middle eddies become symmetric about their shared separating streamline, 'I', (except for the curvature of the lower separating streamline, 'II', and also the difference in velocity profile along that streamline and the upper lid). As a result of this symmetry, the development of the new eddies as A increases occurs between the upper and middle eddies. The sequence is shown in figure 4. In this case, a single interior saddle point on $x = 0$ is not created. Instead, two saddle points lying on streamline 'I' are created when the side eddies appear (figure 4a). As A increases, these approach each other and meet on $x = 0$ at P (figure 4b), creating a parametrically unstable triangular structure. Further increasing A produces a disconnection of this structure, leaving three heteroclinic streamlines spanning the cavity ('I', 'I_1' and 'I_2' in figure 4c), and subsequently the transformation of the saddle points on $x = 0$ to centres, completing the second phase of eddy generation.

As the above discussion shows, during the second phase, the presence of more eddies within the cavity provides more opportunities for local symmetries. However, there are only two types of local symmetry: either the flow within a single eddy is symmetric (as when $S = -1$

or S_2^-), or the flow between two eddies is symmetric (as when $S = S_1^-$). For convenience later, these will be referred to as type 1 and type 2 symmetries respectively. Symmetry in a single eddy (type 1) produces a characteristic pitchfork bifurcation by which the interior saddle point is created, while symmetry over two adjacent eddies (type 2) results in two saddle points on the dividing streamline.

3.2 Sub-cavities and Moffatt eddies

The repetition of the pattern of bifurcation curves in figure 1, and the local symmetries observed, can be explained by considering 'sub-cavities' within the domain, composed of one or more fully-developed eddies and bounded above and below either by one of the lids or by a separating streamline connecting the sidewalls. For example, figure 5(c) shows a cavity containing three fully developed eddies, which form three simple sub-cavities, I, II and III, and also larger sub-cavities such as that formed from the two upper eddies, $I + II$. The speed ratio associated with a sub-cavity is simply the ratio of the fluid speeds along its upper and lower boundaries, and similarly a sub-cavity's aspect ratio is the distance between its upper and lower boundaries divided by the separation of the cavity side walls.

Suppose that in the original single-eddy cavity a flow bifurcation occurs at some combination of speed and aspect ratio, (S^*, A^*), say. From the observations in the previous section, the basic hypothesis here is that the same bifurcation will occur in any sub-cavity whose speed and aspect ratios match S^* and A^*. While it is of course possible to obtain these parameters for each sub-cavity numerically from the streamfunction solution, such an approach would not on its own explain the general relationships between certain parts of the parameter space.

Motivated by the recent work of Wilson *et al.* [19] on stagnation points in shear flows, a better understanding can be developed by recalling some results from Moffatt's work on viscous eddies [16]. In addition to eddies arising in sharp corners, Moffatt also pointed out that a flow generated by an arbitrary disturbance between two infinitely long stationary parallel plates consists of a sequence of equal-size eddies rotating alternately in opposite senses. Moffatt used local extrema in the cross-channel velocity component as a measure of the strength of each eddy, and hence defined a damping factor by considering the relative strengths of adjacent eddies. The value Moffatt found was the same for each eddy pair in the channel, with the numerical value being approximately 353. Moffatt's analysis also yielded a value for the (constant) separation between consecutive eddy centres, and under the non-dimensionalisation in the present work this equates to an eddy aspect ratio of 1.39 — extremely close to the value of A_{eddy} found here computationally.

The example of a disturbance given by Moffatt was a rotating cylinder placed between the plates, however one can see that as A increases, the deep cavities considered here become akin to Moffatt's flow, with the rotating cylinder replaced by the moving lids. Recognising this, it is possible to construct a rough approximation to the flow in a finite cavity by superposing two semi-infinite cavities as shown in figure 5.

The semi-infinite cavity shown in figure 5(a) is driven by the bottom lid, which moves at

(dimensionless) speed 1. Assuming that a constant damping factor σ applies to all eddies (including that adjacent to the lid), the speeds along the separating streamlines (the local extrema) in figure 5(a) will be σ, σ^2, σ^3, etc. Note that for convenience σ is defined as the reciprocal of Moffatt's definition, and is taken to be negative to account for the alternating sense of rotation of the eddies; hence

$$\sigma = -353^{-1} = -2.833 \times 10^{-3}. \tag{5}$$

Similarly, the semi-infinite cavity in figure 5(b) is driven at the top by a plate moving with speed S. Again assuming a constant damping factor, the speeds along the separating streamlines will be $S\sigma$, $S\sigma^2$, $S\sigma^3$, etc. Figure 5(c) shows the superposition of the bottom three eddies of figure 5(a) with the top three eddies of figure 5(b), to produce a rough model of the fluid speeds along the separating streamlines in a finite three-eddy cavity. The σ^3 terms arising on the lids reflect the imperfect nature of the superposition; since σ is very small, these can be neglected for the present purposes. Note also that the curvature of the dividing streamlines is neglected in this simple approximation.

Referring to figure 5(c), and neglecting the cubic terms, it is easy to obtain the following speed ratios:

$$S_I = \frac{S}{\sigma(S+\sigma)}, \tag{6}$$

$$S_{II} = \frac{S+\sigma}{1+S\sigma}, \tag{7}$$

$$S_{I+II} = \frac{S}{\sigma(1+S\sigma)}, \tag{8}$$

where S_{I+II} refers to the speed ratio of the sub-cavity including both the top and middle eddies. When $S = -1$, one can see by inspection that equation (7) gives $S_{II} = -1$, and so the expression is consistent with the global symmetry arising in this case (see discussion in previous section). Considering the sub-cavity $I + II$, rearranging equation (8) gives

$$S = \frac{S_{I+II}\sigma}{1 - S_{I+II}\sigma^2} = S_{I+II}\sigma + O(\sigma^3). \tag{9}$$

Hence, to leading order, if S_{I+II} is to be equal to 1 to produce symmetry, then $S = \sigma$, which from (5) gives $S = -2.833 \times 10^{-3}$. This is almost exactly the value S_1^- described in the previous section, and explains the significance of this particular speed ratio. In a similar way, rearranging (6) gives

$$S = \frac{S_I\sigma^2}{1 - S_I\sigma} = S_I\sigma^2 + O(\sigma^3), \tag{10}$$

and therefore if S_I is to be -1, then $S = -\sigma^2 = -8.03 \times 10^{-6}$. This is close to the value of S_2^- given above, and again provides a connection between the different features of the control space diagram.

Expression (10) is not only useful for finding where partially symmetric conditions arise, but can also explain the shift in the repeated pattern of bifurcation curves in figure 1. The curves

of interest refer to flow transformations that occur in the top eddy (sub-cavity I), with the lower eddies remaining unaffected. The aspect ratio of the top eddy is therefore given by

$$A_I = A - 2A_{eddy}. \tag{11}$$

A bifurcation that occurs in the first phase at (S^*, A^*) will be repeated in the top eddy during the second phase if $A_I = A^*$ and $S_I = S^*$. From (10) and (11) this will happen when

$$\begin{aligned} A &= A^* + 2A_{eddy}, \text{ and} & (12)\\ S &= S^*\sigma^2. & (13) \end{aligned}$$

Of course on the logarithmic scale of figure 1, equation (13) corresponds to a horizontal linear shift, since (13) becomes $\log|S| = \log|S^*| + 2\log|\sigma|$. Hence the horizontal and vertical shifts in the repeated pattern are explained by Moffatt's analysis.

The only curves in the shaded region in figure 1 that are not perfect repetitions of the first phase curves are SE_2 and SN_2 in the vicinity of points B^* and C^*. The reason for this is that in the first phase, the corresponding portion of the bifurcation curves SE_1 and SN_1 lie in a region of parameter space where $A < A_{eddy}$, i.e. the cavity aspect ratio is less than the typical aspect ratio of a fully-developed eddy. A different sequence of bifurcations occurs as $A \to 0$, and the simple analysis above is not valid in this parameter range.

In cavities deeper than those considered here, i.e. in the third and subsequent phases of eddy generation, it is expected that the curves in the shaded part of figure 1 will be exactly reproduced, shifted vertically by $2A_{eddy}$ and horizontally by $2\log|\sigma|$. Indeed it is straightforward to generalise the relations (12) and (13) to cavities containing N_e eddies:

$$\begin{aligned} A &= A^* + (N_e - 1)A_{eddy}, & (14)\\ S &= S^*\sigma^{N_e - 1}. & (15) \end{aligned}$$

These only relate to bifurcations in the top eddy, adjacent to the top lid; this pattern will only repeat once per phase of eddy generation (in the range $-1 \leqslant S < 0$ — other repetitions will occur outside this range, see later). The flow development in the other eddies/sub-cavities will produce repetitions of the second-phase curves between S_0^- and S_2^-, and these will repeat numerous times, as the development of more eddies provides more sub-cavity permutations and more opportunities for local symmetries within them. The speed ratios at which these symmetries arise are connected to the factor σ by the relationship

$$S_i^- \approx -|\sigma|^i \quad i = 0, 1, 2, \ldots \tag{16}$$

4 Lids Moving in the Same Direction

So far only negative lid speed ratios have been considered, and for such values the cavity contains an odd number of eddies. Speed ratios in the range $0 < S \leqslant 1$ are now considered, where the lids move in the same direction, and the cavity contains an even number of eddies.

Even when A is small, there are still two eddies in the cavity, albeit wide, thin ones. Since it has not been considered before, the small-A part of the control space is shown in figure 6. The bifurcation curves show a very similar structure to those seen by Gaskell *et al.* [1,20] in cavities with free-surface side walls. As $A \to 0$ increasingly intricate sequences of nested three-eddy separatrices develop in each of the two main eddies. These chains of stagnation points have recently been explored in a general context by Wilson *et al.* [19]. The key difference in the control space for the present, solid-walled cavity is the existence of curves SE_1 and SN_1. These correspond to the appearance of side eddies on the solid walls and the appearance of two small, off-centre secondary eddies by means of saddle-node bifurcations. Neither of these features is seen in the free-surface cavities.

The focus of the present paper, however, is deep cavities, and the main part of the $0 < S \leqslant 1$ control space is presented in figure 7. Two phases of eddy generation are shown. Comparing this figure with figure 1, one can see the now familiar patterns of bifurcation curves repeated (albeit reversed due to the change in sign of S) in figure 7. Again there are particular values of S where the bifurcation curves exhibit local symmetry, and this is again a result of type 1 or type 2 symmetry within parts of the cavity. Computationally, the values of the special speed ratios are found to be

$$\begin{array}{lcll} S_0^+ & = & 1, & \text{(type 2)} \\ S_1^+ & = & 2.84 \times 10^{-3}, & \text{(type 1)} \\ S_2^+ & = & 8.5 \times 10^{-6}, & \text{(type 2)} \\ S_3^+ & = & 2.5 \times 10^{-8}, & \text{(type 1)} \end{array}$$

and once again the significance of the velocity damping factor $\sigma = -2.833 \times 10^{-3}$ is seen, since

$$S_i^+ \approx |\sigma|^i \quad i = 0, 1, 2, 3, \ldots \tag{17}$$

For this range of S, the additional eddy at the bottom of the cavity plays no part in the eddy genesis, but its presence does shift the entire bifurcation pattern vertically upwards by a distance of A_{eddy}. It is clear that the whole (reflected) bifurcation pattern of figure 1 is also shifted to the left in figure 7 due to the additional eddy, and it is no surprise that the size of this shift is $\log|\sigma|$. Suppose there are N_e ($\geqslant 2$) eddies in the cavity. The cavity can be split into two sub-cavities: one consisting of the bottom eddy only, and the other containing the remaining $N_e - 1$ eddies. Since the bottom eddy is passive, the upper sub-cavity behaves just as described in the previous section, where $S < 0$. However, the speed ratio of this sub-cavity is given by the ratio of the upper lid speed to the speed along the dividing streamline between the two sub-cavities. The superposition approach of figure 5 can be used to obtain an approximate value of the latter speed: the bottom lid will contribute σ and the top lid will contribute $S\sigma^{N_e-1}$, giving a speed ratio for the upper sub-cavity of

$$S_{sc} = \frac{S}{\sigma + S\sigma^{N_e-1}}. \tag{18}$$

Rearranging this for S gives

$$S = S_{sc}\sigma + O(\sigma^{N_e}), \tag{19}$$

revealing the universal scaling factor once again.

A consequence of this shift is the addition of the shaded section of figure 7, which contains a repeat of the pattern associated with type 2 symmetry in part of the cavity. This is because there is now an even number of eddies, and therefore no middle eddy, so when the cavity becomes completely symmetric (at $S = 1$), the symmetry in the middle of the cavity is about the central dividing streamline.

5 Conclusion

The development of eddies in deep double-lid driven rectangular cavities has been explored in an extension of the previous work by Gürcan *et al.* [12] (referred to as 'Part 1'). The extended control space diagram for $-1 \leqslant S < 0$ reveals that the pattern of bifurcation curves observed in Part 1 is repeated almost exactly in a 'second phase' of eddy generation, at higher aspect ratios and at a shifted range of speed ratio. As A increases through the second phase, the number of eddies in the cavity increases from three to five, and the aspect ratio of the fully developed eddies is found computationally to be $A_{eddy} = 1.38 \pm 0.05$. This is in good agreement with the value of 1.39 obtained from Moffatt's [16] analysis of the eddy flow generated by an arbitrary disturbance between infinite stationary parallel plates. In the cavity flow, the motion of each lid essentially becomes an example of a 'disturbance' driving the flow. Exploiting this similarity with Moffatt's flow, the superposition of two semi-infinite cavities produces a crude but surprisingly accurate model of the flow in a finite double-lid driven cavity.

The Part 1 bifurcation curves repeat in the second phase because any bifurcation that occurs in the single-eddy cavity of Part 1 also occurs in the uppermost eddy of a multi-eddy cavity when the eddy's local speed ratio and aspect ratio match those of the original bifurcation. Assuming a constant velocity damping factor, σ, as found by Moffatt, the superposition model allows the speed ratios of individual eddies to be calculated simply, and demonstrates that the bifurcations of Part 1 will repeat in the top eddy at speed ratios which are smaller than the original by a factor of σ^{N_e-1}, where N_e is the number of eddies in the cavity.

In addition to the repeated pattern, a new, locally symmetric, pattern of bifurcation curves is identified, which was not present in Part 1. This is associated with symmetric flow conditions between two of the eddies within the cavity. Other speed ratios producing local symmetries within an individual eddy are also identified. All the speed ratios producing partial symmetry in the cavity are integer powers of Moffatt's velocity damping factor.

Control space diagrams are also presented for the case when the lids move in the same direction, and therefore $S > 0$. In this case the whole $S < 0$ bifurcation pattern is seen again, but reflected due to the change in sign of S. However, the presence of an additional eddy in the cavity when $S > 0$ means that the pattern is shifted to higher aspect ratios by a distance of A_{eddy}, and to smaller speed ratios, again by a factor equal to Moffatt's velocity damping factor.

This work completes the study of Stokes flow transformation and eddy generation in double-lid driven cavities. At higher aspect ratios the new patterns of bifurcation curves identified here and those in Part 1 will repeat at values of S and A which produce appropriate conditions within individual eddies or parts of the cavity. At higher speed ratios, i.e. $|S| > 1$, the same bifurcation patterns will also appear again, as this is essentially just an inversion of the domain and a rescaling of the velocity field.

Acknowledgements: This work was supported by the TUBITAK in Turkey.

References

[1] Gaskell, P. H., Gürcan, F., Savage, M. D. and Thompson, H. M. Stokes flow in a double-lid-driven cavity with free surface side-walls. *Proc. Instn Mech. Engrs. Part C, J. Mechanical Engineering Science*, 1998, **212**, 387-403.

[2] Aidun, C. K., Triantafillopoulos, N. G., and Benson, J. D. Numerical study of viscous flow in a cavity. *Phys. Fluids (A)*, 1991, **3**, 2081-2091.

[3] Canedo, E. L. and Denson, C. D. Flow in driven cavity with a free surface. *Am. Inst. Chem. Engrs. J.*, 1989, **35**, 129-138.

[4] Helebrand, H. Tape casting. In: *Processing of Ceramics, Part 1*, (Ed. R. J. Brook), 1989, VCH Publisher.

[5] Higdon, J. J. L. Stokes flow in arbitrary two-dimensional domains: Shear flow over ridges and cavities. *J. Fluid Mechanics*, 1985, **159**, 195-226.

[6] Jeffrey, D. J. and Sherwood, J. D. Streamline pattrns and eddies in low Reynolds number flow. *J. Fluid Mechanics*, 1980, **96**, 315-334.

[7] Weiss, R. F. and Florsheim, B. H. Flow in a cavity at low Reynolds number. *Phys. Fluids*, 1965, **8**, (9), 1631-1635.

[8] Sturges, L. D. Stokes flow in a two-dimensional cavity with moving end walls. *Phys. Fluids*, 1986, **29**,(5), 1731-1734.

[9] Chien, W. L., Rising, H. and Ottino, J. M. Laminar mixing and chaotic mixing in several cavity flows. *J. Fluid Mechanics*, 1986, **170**, 355-377.

[10] Jana, C. M., Metcalfe, G. and Ottino, J. M. Experimental and computational studies of mixing complex Stokes flows: the vortex mixing flow and multicellular cavity flows. *J. Fluid Mechanics*, 1994, **269** , 199-246.

[11] Gürcan, F., Deliceoğlu, A. and Bakker, P. G. Streamline topologies near a non-simple degenerate critical point close to a stationary wall using normal forms. *J. Fluid Mechanics*, 2005, **539** , 299-311.

[12] Gürcan, F., Gaskell, P. H., Savage, M. D. and Wilson, M. C. T. Eddy genesis and transformation of Stokes flow in a double-lid driven cavity. *Proc. Instn. Mech. Engrs. Part C, J. Mechanical Engineering Science*, 2003, **217**, 353-364.

[13] Bakker, P. G. *Bifurcations in Flow Patterns.* 1991, (Kluwer Academic, Dordrecht, The Netherlands.)

[14] Brøns, M. and Hartnack, J. N. Streamlines topologies near simple degenerate critical points in two-dimensional flow away from boundaries. *Phys. Fluids*, 1999, **11**(2), 314-324.

[15] Gürcan, F. Streamline topologies in Stokes flow within lid-driven cavities. *J. Theor. Comput. Fluid Dynamics*, 2003, **17**(1), 19-30.

[16] Moffatt, H. K. Viscous and resistive eddies near a sharp corner. *J. Fluid Mechanics*, 1964, **18**, 1-18.

[17] Joseph, D. D. and Sturges, L. The convergence of biorthogonal series for biharmonic and Stokes flow edge problems: Part II. *SIAM. J. Appl. Math.*, 1978, **34**, 7-27.

[18] Smith, R. C. T. The bending of a semi-infinite strip. *Austral. J. Sci. Res.*, 1952, **5**, 227-237.

[19] Wilson, M. C. T., Gaskell, P. H. and Savage, M. D. Nested separatrices in simple shear flows: the effect of localized disturbances on stagnation lines. *Phys. Fluids*, 2005, **17**, Art. No. 093601.

[20] Gaskell, P. H., Savage, M. D. and Wilson, M. Stokes flow in a half-filled annulus between rotating coaxial cylinders. *J. Fluid Mechanics*, 1997, **337**, 263-282.

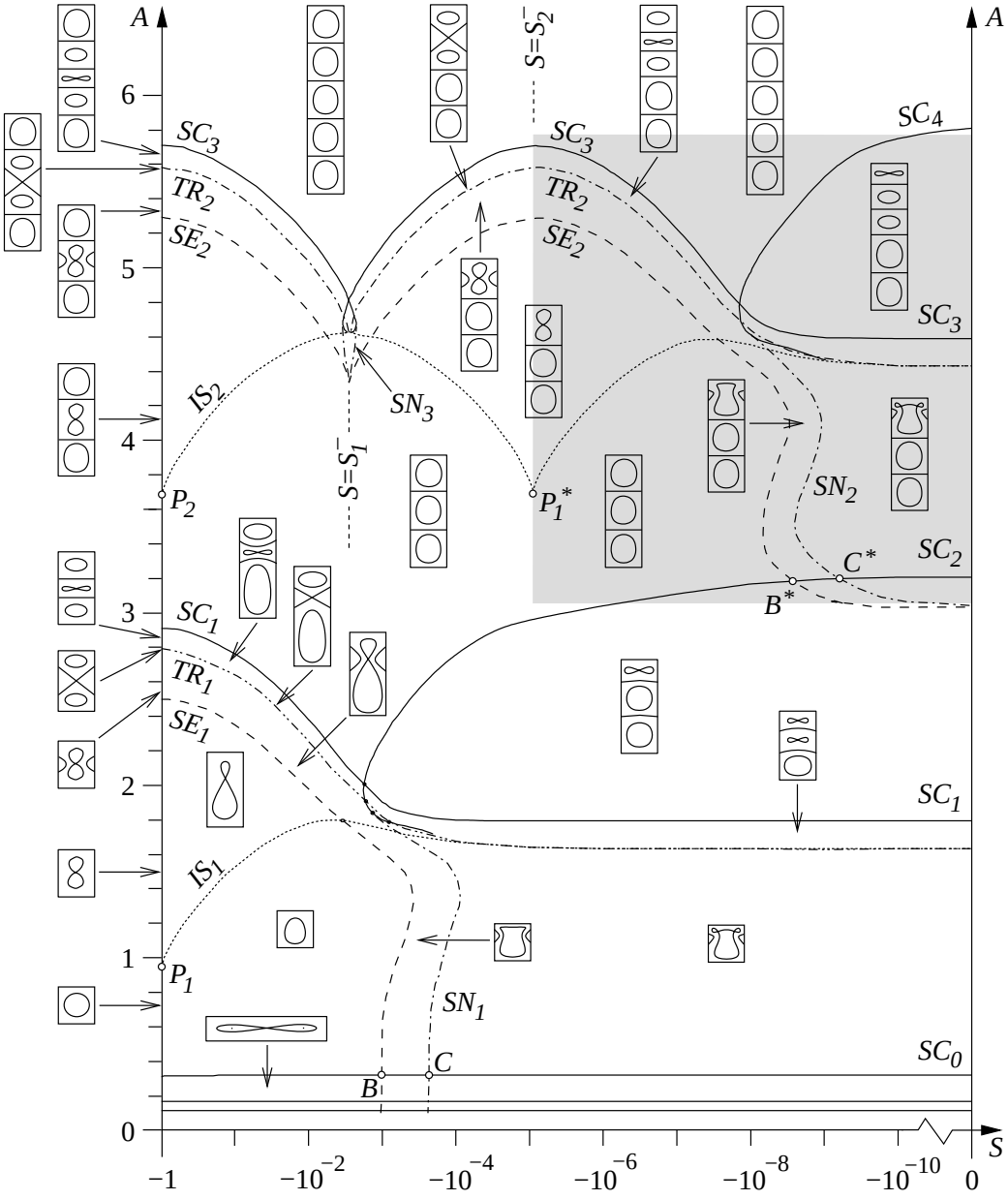

Figure 1: Extended control space diagram for a double-lid-driven cavity with solid walls, with $-1 \leqslant S < 0$, and $0 < A \leqslant 6$. The curves show the combinations of the control parameters at which key flow transformations arise. Schematics show typical flow structures in the various regions.

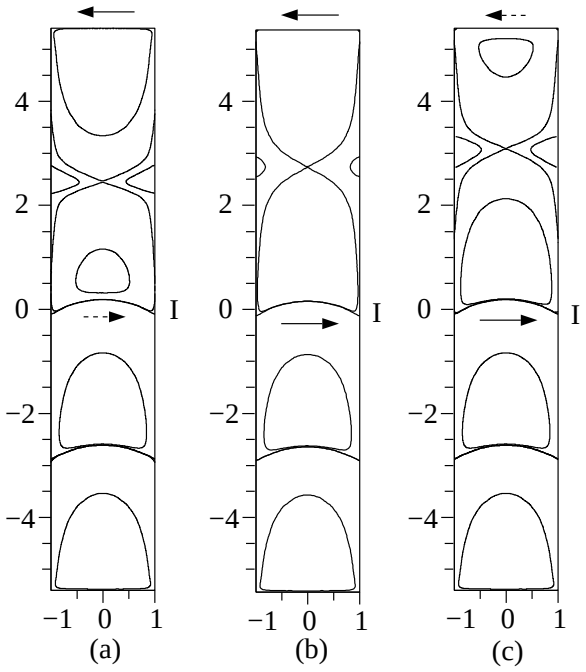

Figure 2: Streamlines showing the structure of the flow when $A = 5.4$ and (a) $S = -9\times10^{-5}$, (b) $S = S_2^- = -8.5 \times 10^{-6}$, and (c) $S = -9 \times 10^{-7}$. In case (b) the flow is symmetric in the top half of the cavity, apart from the curvature of the separating streamline 'I'.

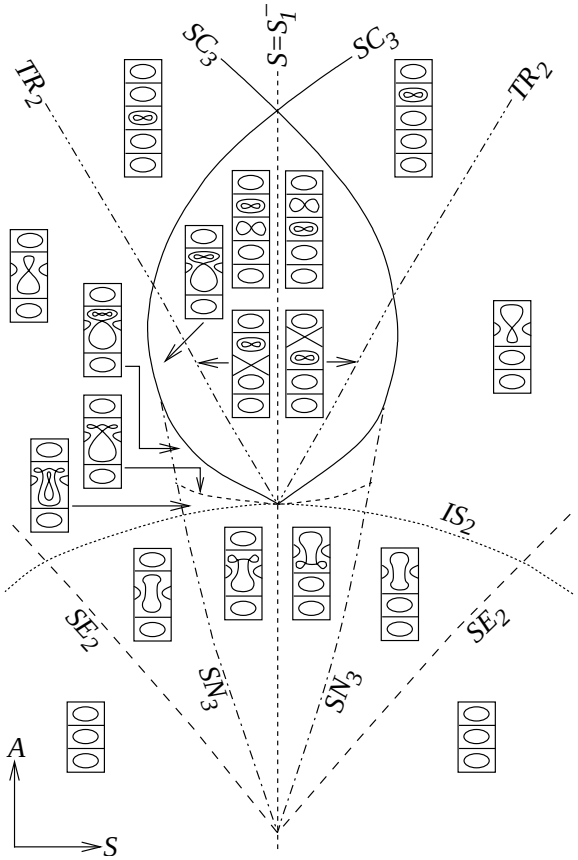

Figure 3: Enlarged view of the control space near $S = S_1^- = -2.84 \times 10^{-3}$, where the bifurcation curves exhibit local symmetry. The schematics illustrate the flow patterns associated with each region, and show how the flow pattern in the upper half of the cavity is inverted on either side of $S = S_1^-$.

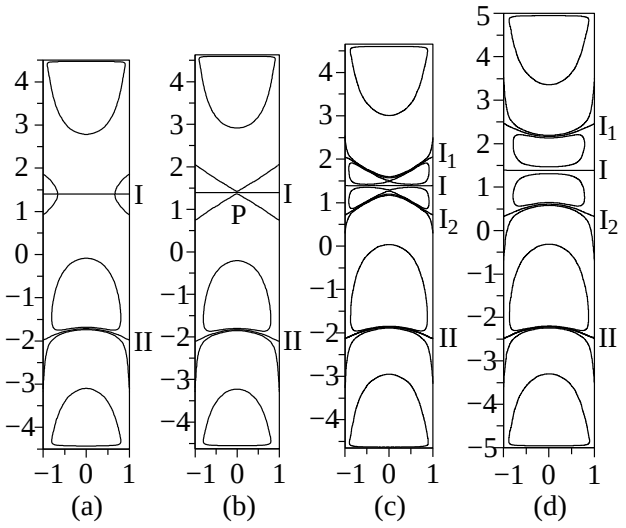

Figure 4: Streamlines showing the transformation of the flow when $S = S_1^- = -2.84 \times 10^{-3}$ and A increases: (a) $A = 4.5$, (b) $A = 4.6253$, (c) $A = 4.65$, (d) $A = 5$. Notice how the flow above the bottom eddy is symmetric about the separating streamline 'I', apart from the curvature of streamline 'II'.

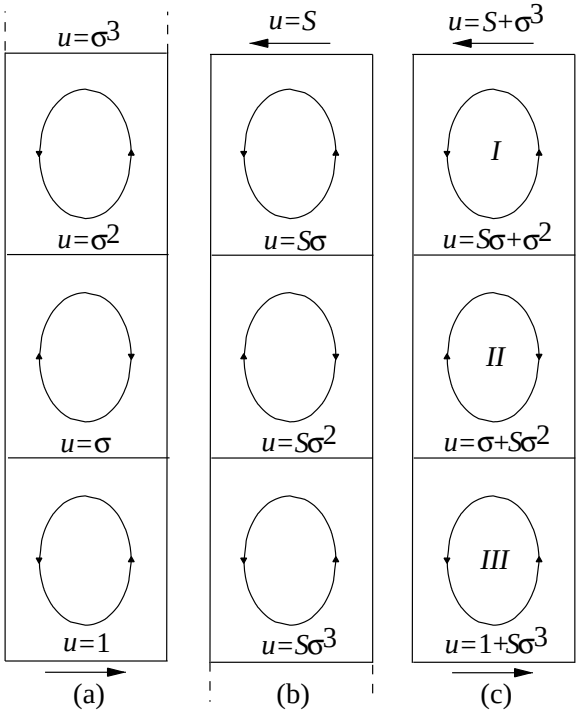

Figure 5: A superposition of two semi-infinite cavities to produce an approximate solution for the flow in a three-eddy finite cavity.

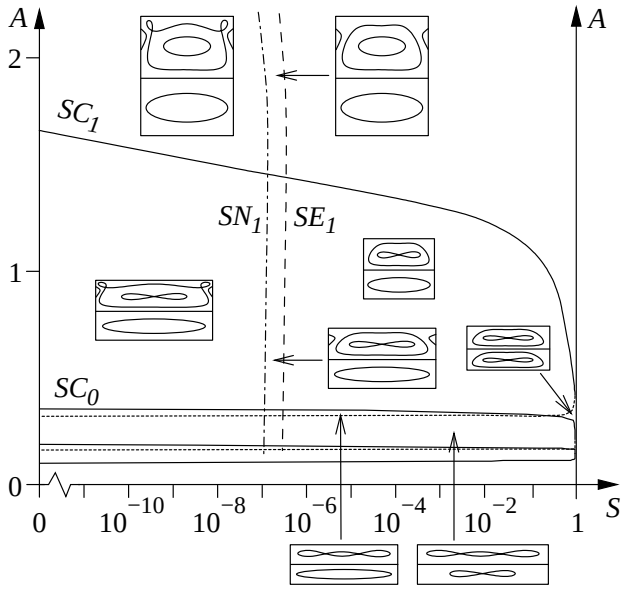

Figure 6: The lower part of the control space when the driving lids move in the same direction, i.e. when $0 < S \leqslant 1$ and $A < 2$.

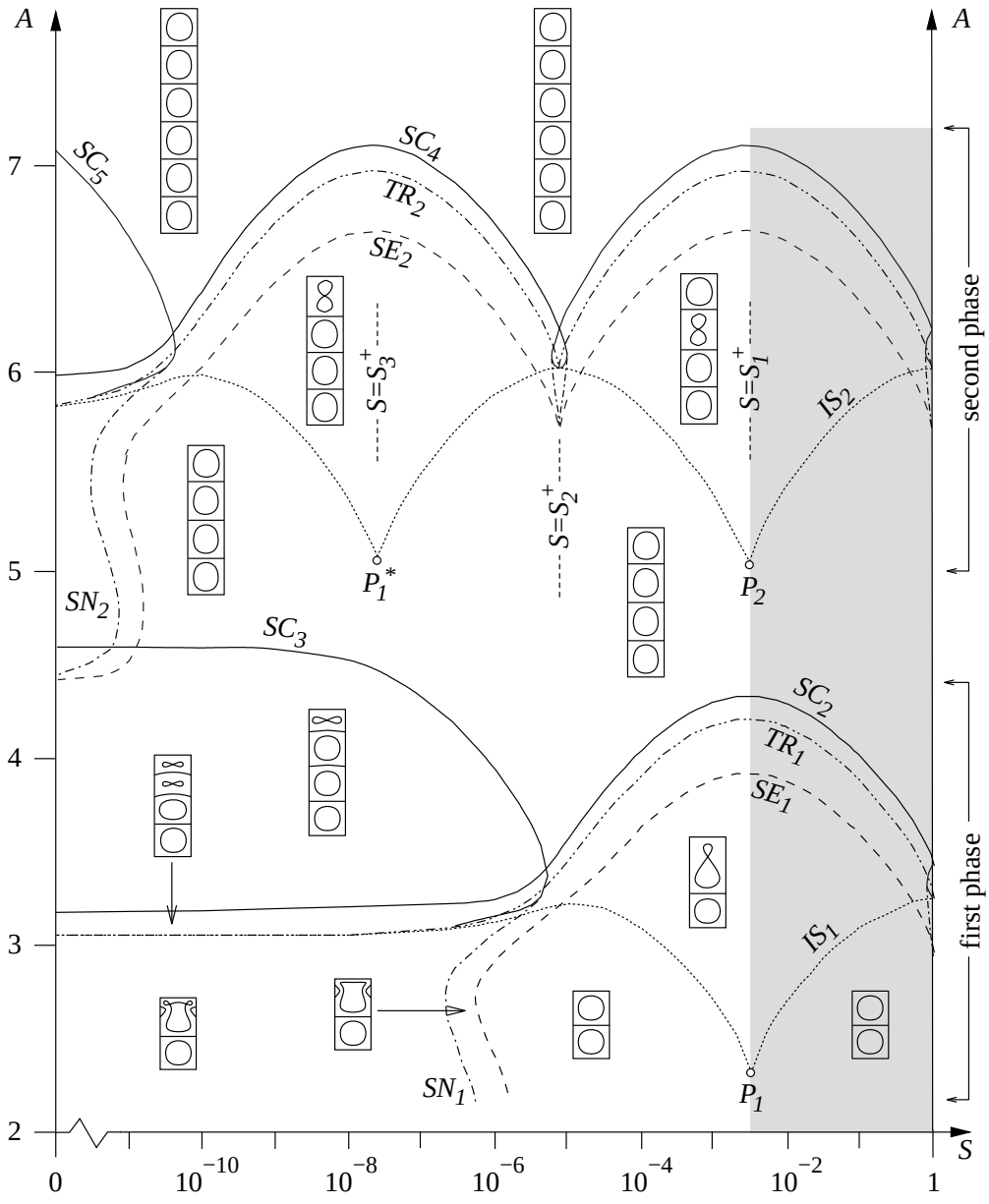

Figure 7: Control space diagram showing the first and second phases of eddy generation when the driving lids move in the same direction, i.e. when $0 < S \leqslant 1$.